Abstract This paper presented a semi-automatic framework dedicated to vessel segmentation for 3-D coronary artery Computed Tomography Angiography (CTA) sequence. The segmentation scheme consists of two part: centerline extraction and vessel surface recovering. First, spherical flux and minimal path method was employed to extract the centerlines. To implement automatic centerline extraction starting from the second frame, a novel method for detecting stable key points was proposed and 3-D SIFT descriptor was used for key point description. In this process, the key points on distal vessel are easily mismatched. A centerline tracking algorithm based on patient-specific vessel model was used to complete the extraction. The the overlap (OV) result of proposed framework is 93.56% (LAD), 90.96% (LCX) and 93.76% (RCA). We achieved accuracy (AC) result: 0.6508 mm (LAD) 0.6141mm (LCX) and 0.6297 mm (RCA) within the image voxel size (0.68mm).
Keywords :

Introduction

Lung cancer accounts for the highest incidence and mortality rates among all kinds of cancer worldwide [1]. Thus, precision treatment for lung cancer is in significant demand. Radiation therapy (RT) has become one of the main treatment for lung cancer second only to surgery. To implement high precision radiation therapy, image guided radiation therapy (IGRT) was commonly used [2]. In the process of radiation therapy for pulmonary tumor, coronary artery is one of the most vulnerable tissue. Once exposed to radiation beyond normal dose, radiation heart diseases can be caused. Quantitative description of coronary artery motion can be used for planning circumvent strategy and also for diagnosing and treating cardiovascular disease (CVD).

The motion of coronary artery is effected by both heart beating and respiration. And its movement and deformation are heterogeneous during a cardiac cycle [3]. In early works, X-Ray angiography is the main technique for visualizing the motion of the coronary arteries. And coronary motion is tracked in 2-D projection images, which is limited by the overlap of vessels [4]. In order to recover the 3-D motion information of coronary artery, the 3-D coronary tree is reconstructed for each cardiac phase in [4][5][6]. These days, due to the advance in 3-D echography, cine-MRI, and multislice computed tomography (MSCT), the 3-D CTA is available for describing the motion of full cardiac structures [8].

Few works have been devoted to the characterization of coronary artery motion. A detailed discussion on the global and local coronary artery motion features was given in [7]. The displacement and 3-D velocity of the landmarks were analyzed in [8] from MSCT angiography. A template matching method was used in modeling coronary artery motion in [9]. While in those works, coronary centerline extraction was carried out repeatedly for each phase in a cardiac cycle. The correlation between adjacent phase has not been employed to improve the effectiveness of the extraction method.

Accurate extraction of coronary centerlines is an important step for assessing the motion of coronary artery. Numerous methods has been presented for extracting coronary centerlines for 3-D CTA. Early reviews of 3-D vessel segmentation techniques can be found in [10][11]. In recent works, a machine learning-based framework for vessel segmentation [12] has outperformed the widely-used hessian-based vesselness [13] and optimally oriented flux (OOF) [14]. A graph-based method using tubularity Markov tree (TMT) was proposed in [20]. This method is proved to be more accurate and time efficient than some classical graph-based methods. For challenging image quality conditions, a generic curvature based vessel segmentation method [21] was proposed to segment the vessels by minimizing surface curvature. Example-based segmentation and component-tree were used in the extracting cerebral vascular networks [22], which has taken the advantage of expertise of the clinician to avoid possible errors. However, when the temporal dimension is added, selecting a few seed points manually for each frames could be a rather laborious task for semi-automatic extraction. Besides, the image quality of 3-D CTA sequence could be unstable due to the presence of different levels of movement artifacts. A robust and efficient vessel segmentation method dedicated to 4-D CTA, i.e. 3-D CTA sequence, is lacked.

This paper presented a semi-automatic scheme for coronary artery centerline extraction and matching. For each frame, the main coronary centerlines are extracted by a minimal path method with intermediate point. A direct vessel tracking was presented to improve the overlap accuracy of the extraction suffering from the failure of the key point matching for distal vessels. The main contribution of this work are: 1) A simple method for recovering the vessel surface is presented. It performed well in removing surrounding cardiac structure and small branches of the main coronary vessels. 2) 3D SIFT descriptor was used for key point description and a novel method for detecting stable key points is presented. 3) A direct tracking algorithm based on patient-specific vessel model was presented for distal vessel tracking.

Methodology

A novel Coronary Artery vessel segmentation framework

The main motivation of this work is presenting a semi-automatic segmentation approach for 3-D coronary CAT sequence with only a few user interactions in the first frame, while similar procedures are proceeded automatically for subsequent frames. In order to characterize the motion of coronary artery, the correspondences between key points in adjacent frames are established. The segmentation contains two stages: centerline extraction and vessel surface recovering. First, two endpoints and several intermediate points of the main coronary vessels, i.e. left anterior descending artery (LAD), left circumflex artery artery (LCX), and right coronary artery (RCA) in the first frame of the sequence are manually selected as the input of the scheme. The coronary artery centerlines are then extracted using a flux-based filter and minimal path method solved by fast marching algorithm [15]. In similar way, centerlines of subsequent frames are extracted with automatically matched points. A novel stable key point detection method was proposed to select a set of key points on an extracted centerline. The key points are described by 3-D Scale-Invariant Feature Transform (SIFT) descriptor [16]. To solve the problem of unreliable matching for distal vessels, we introduced a tracking method to complete the extraction. The workflow of the scheme is organized as follows:

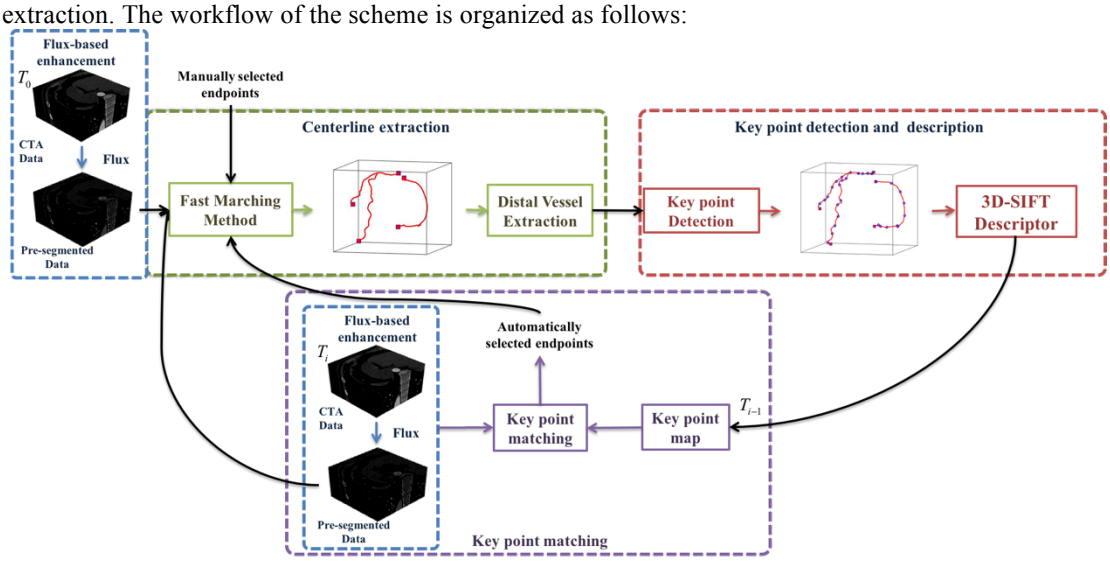

Figure 1 Coronary Artery vessel segmentation framework

Centerline-based coronary artery segmentation

Among centerline-based vessel segmentation methods, minimal path approaches are particular popular [10]. The extraction of the constrained two-point centerline is performed by minimizing the cumulative cost measure $\tilde{P}(C(s))$ along the path C. Such minimization model can be solved by either graph-based methods such as Dijkstra algorithm [17] or fast marching algorithm [15], where the global optimal is guaranteed to be found [19]. This leads to its main advantage of passing through occlusions, bifurcations, regions unrecognizable from surrounding cardiac structures and regions suffer from bad image quality [19]. The minimal path of the given endpoints p_0 and p is defined as:

$$U_{P_0}(p) = \inf_{C(0)=p_0;C(L)=p} E(C) = \inf_{C(0)=p_0;C(L)=p} \int_0^L \tilde{P}(C(s))ds$$

In this paper, the minimal path is determined by solving the Eikonal equation, i.e. $\left\|\nabla U_{P_0}\right\| = \tilde{P}$ with $U_{p_0}(p_0) = 0$ [23] using fast marching algorithm [15]. Compared to other deformable models such as snake, minimal path method is more time efficient and easier to implement [23]. However, the main disadvantage of this method is the occurrence of "short cut", i.e. the path went to surrounding structure somewhere and returns to the endpoint later, which can hardly be robustly avoided by the choice of cost metric. To improve the robustness of minimal path method, additional intermediate points can be added to divide the path into subpaths [19]. To this end, the intermediate points are manually selected only in the starting frame, and the multiple-point minimal path was proceeded automatically in subsequent frames.

A common choice of cost metric is the reciprocal of vessel-specific features [10], such as hessian-based vesselness [13] and flux-based medialness [14]. In this work, we simply employed flux-based medialness as the cost metric. Flux-based segmentation method has been proved to work well in extracting thin and low-contrast vessels [14][24][25]. As a mathematical concept, flux can be computed as the integral of the gradient flux over a closed boundary. In particular, the flux in a spherical surface is referred as spherical flux [14]:

$$flux(p,r) = \int_{\partial\Omega} < \vec{v}, \hat{n} > dS = \int_{\Omega} \nabla I dv$$

where $\partial\Omega$ is a closed spherical boundary of region Ω with radius r, $\hat{n}$ is the outward radial normal of C. $\vec{v}$ is the gradient vector field of a volume I, which can be obtained by convolving the volume with the Gaussian derivatives as $\vec{v} = \nabla(G * I) = \nabla(G) * I$ [14]. By apply the divergence theorem, flux is calculated as the integral of divergence of the volume. The multi-scale analysis of spherical flux is achieved by giving a set of radiuses, and choosing the optimal flux response. The optimal scale $r(p)$ is not necessarily equal to the theoretical radius [24]. In Fig. 5 below, we presented the maximum intensity projection (MIP) view of the pre-segmentation result.

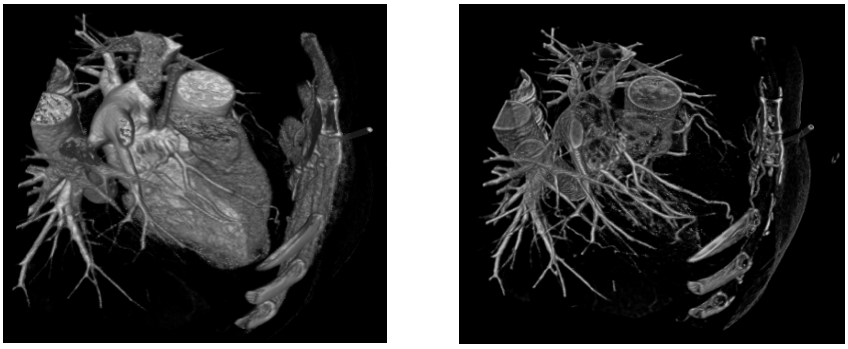

Figure 2 Illustration of the flux responses on our cardiac CT data. Left to right: original, spherical flux.

After equidistance resampling, an extracted centerline is denoted as $P = \{p_1, p_2, \ldots, p_N\}$. To segment the full vessel structures, we proposed a simple method to recover the vessel surface from the extracted centerline. First, the local direction of centerline at point p_i is estimated as $v_i = \frac{p_i - p_{i-1}}{|p_i - p_{i-1}|}, i = 1,2,\ldots,N-1$, which is assumed to be the vessel's principal direction. From the cross-section view of centerline point, the vessel region is selected by $V_t = V_i \cap V_d$. Region V_i is defined as the connected region around the center point by a fixed threshold calculated as $\frac{|I(p_i) - I(x,y)|}{I(p_i)} < T$. Region V_d is determined by the angle between the local direction and principal direction, calculated as $\frac{v_i \cdot v(x,y)}{\|v_i\| \|v(x,y)\|} < \theta$. The local vessel orientations $v(x,y)$ were estimated using hessian matrix by taking the eigenvector of the smallest eigenvalue. Compared to intensity-based method, this method is more robust for removing small branches and adjacent cardiac structures, which is showed in Fig 3 (2). Local vessel radius r_i is estimated by the average of the minor axis length $L_{min}$and major axis length L_{maj} of the segmented region marked in red point in Fig.3 (1) as $R = (L_{min} + L_{maj})/2$.

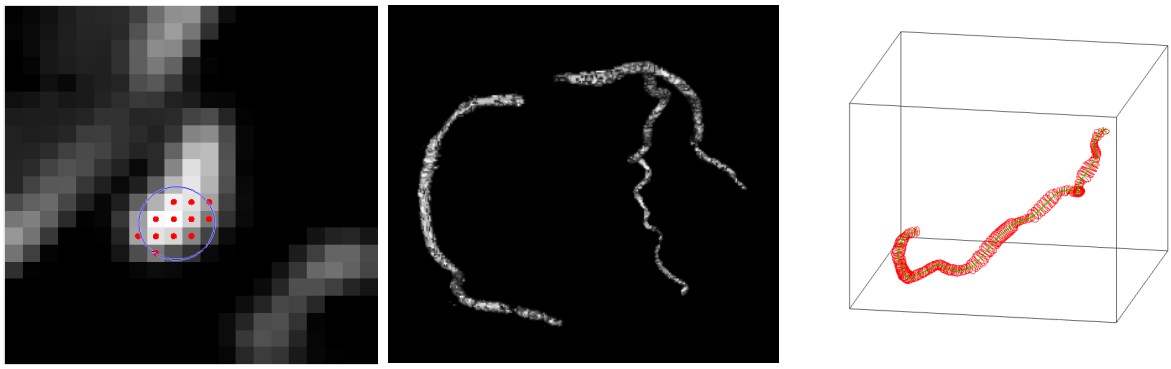

Figure 3 (1)Vessel segmentation from cross-sections view. (2)Recovered Vessel surface. (3)Local vessel radius estimation of LAD (coronary ostium is in the lower place).

To build a patient-specific vessel model**,** vessel surface is represented by its centerline points P, associated radiuses R and intensity of the cross-section center I denoted as $X(P(l), R(l), I(l), t)$. After each centerline extraction, the radiuses and central intensity are updated by $x_t = \tau x_{t-1} + (1-\tau)x_t$. The distance to the coronary ostium l is used to index the points. An illustration of the reconstructed LAD by its centerline points and associated radiuses is given in Fig 3. (3).

Key point description, detection, and matching

Key point description is of great importance for realible key point matching. We applied 3D SIFT descriptor to describe the local properties of a key point, also known as the feature vector $v(p)$ [16],

which is formed by the orientation histograms of given subregions [26]. The orientation assignment and gradient histogram presented in [16] was used. The spherical window is centered at the key point with radius 2σ. And it was divided into 4×4×4 cubic subregions. (Figure 2.) For each point in a subregion, the orientation is assigned using regular icosahedron with 12 vertices bins. When a gradient vector intersect with a triangle tile, the vector is then interpolated to the three vertices with the weight of the distance between the intersection and the vertices. So the feature vector is $4\times4\times4\times12 = 768$ in length, which ensures the distinctiveness of the feature of a given point.

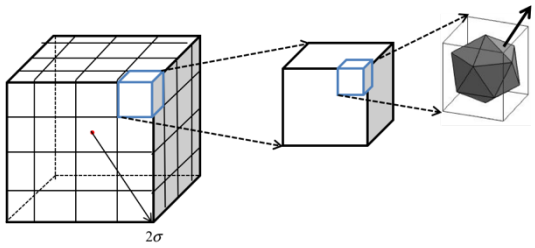

Figure 4 Computation of 3D SIFT descriptor

Reliable key points for point matching should have highly distinctive local properties and be stable landmarks changing over time. Regular tube-like structure is almost invariant along axis direction and thus is considered as poorly-localized object [16], while irregular tube-like structures such as bifurcation and bent locations can be seen as stable landmarks. Detecting those structures respectively is a nontrivial problem. Since the detection is carried out after centerline extraction, we selected the key points direct on the extracted centerlines. A novel method was proposed to detect stable landmarks on the centerline, and the key points are chosen from the local maxima of the array $M(i), i = 1, \ldots, N(\mathrm{t})$:

$$M(i) = \sum_{p \in C} 1 \cdot (Flux(p) > \eta)$$

Region C is a sphere centers in $p_{t,i}$ with a fixed window size w. The operation $1 \cdot (condition)$ returns 1 if the condition is satisfied, else returns 0. Local maxima are filtered by minimum peak width w_{min} and minimum peak prominence h_{min} (a minimum vertical drop to both sides). And the number of key points is highly dependent on the choice of w_{min} and h_{min}.

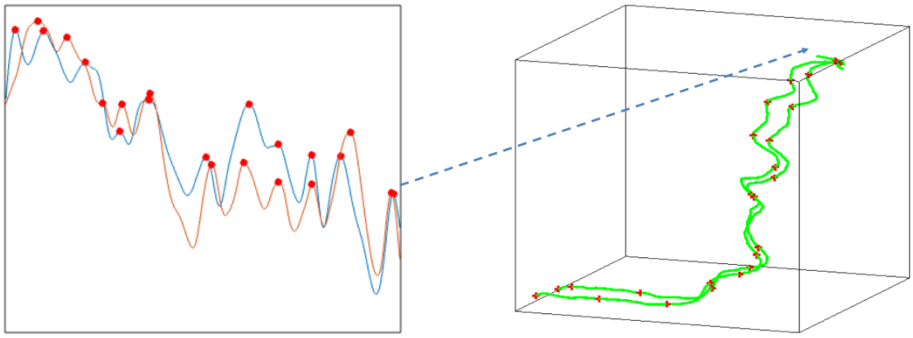

Figure 5 key point selection and matching

On the extracted centerlines of two adjacent frames, as showed in Fig. 5, most detected key points can easily find its correspondence by the length to the ostium. Selected Maxima forms a key point set $S_t = (q_{t,1}, q_{t,2}, \ldots, q_{t,M(t)})$,$1 \le t \le F$. Key point sets are used to generate feature vectors $u(q_{t,k})$ for the matching between frame t and frame t+1. Due to occlusion, bad image quality or the fail of detection, at frame t, there is at most t feature vectors describing the same key point $q_{t,k}$, the feature vector u is selected by:

$$u(q_{t,k}) = \underset{v(q_{i,k}),1 \le i \le t}{\operatorname{argmin}} \left(\sum_{j=1}^{t} \left\| v(q_{i,k}) - v(q_{j,k}) \right\| \right)$$

This provide an estimation for the average of the feature vectors, which improved the robustness of the key point description. The propagation for the key point set S_t to frame t+1 is carried out by a searching procedure. We used the flux pre-segmented volume as a mask of the search space. The optimal match is determined by the the minimum distance $S(p,q)$, and those with $S_{min}\ (p,q) > \alpha$ are considered as unreliable match. The similarity between a key feature point q and a point p in the search space is measured by the Euclidian distance of the feature vectors.

$$S(p,q) = \|u(q) - v(p)\|$$

The reliably matched key points are used as endpoints and intermediate points for centerline extraction at frame t+1. Meanwhile, the key point sets were constructed to represent the correspondences of the vessel centerlines.

A direct tracking algorithm for distal vessels

Distal vessels are thin and low-contrast part at the end of the vessel tree and can hardly be matched reliably. We presented a direct tracking algorithm to complete the extraction for distal vessels. Most direct centerline tracking algorithms are initialized with one seed point, and tracking iteratively along the vessel by predicting the successive centerline position. A major drawback of these algorithms is that the tracking process may end prematurely for imaging artifacts [10]. We improved its robustness by incorporating patient-specific vessel model for point position recentering. The termination of the tracking algorithm is determined by the vessel centerline length. The pseudo-code of the tracking algorithm is provided in Fig 6. For each step, the vessel direction v_p is determined by hessian matrix eigenvectors. We chosen a small constant d_0 as the displacement in order to deal with the large variations of the vessel curvature. The recentering scheme is applied on the cross-section perpendicular to direction of the pervious point inside a circular window. The center of gravity for the pixels with $I(x,y) > I(l)$ was estimated as the center of the cross-section. We chosen the window size from the vessel radius $R(l)$.

Algorithm: $DirectCenterlineTracking(p_0, d_0, VL)$

begin

$vl \leftarrow 0$

$p \leftarrow p_0$

while $l < VL$

$v_p \leftarrow V(p)$

$x \leftarrow x + v_p \cdot d_0$

$x \leftarrow recenter(x)$

$q(end+1) \leftarrow x$

$l = l + \|x - q(end)\|;$

end

end

Figure 6 . Direct centerline tracking for distal vessels

Experiment

Proposed method was evaluated on our 4-D CTA dataset with manually rectified ground truth . The CTA sequence was acquired at 21 evenly-spaced phases in a cardiac cycle. The original volume size is $512\times512\times227$. The voxel size is $0.68\times0.68\times0.5\ mm^3$. We used linear interpolation to equalize the pixel size and slice thickness.

The starting point of a centerline is set on the center of the coronary ostium and the end point is set at the most recognizable distal point of the main vessels (LAD, LCX, RCA). Left anterior descending artery (LAD) and left circumflex artery (LCX) shares the starting point. Thus, only 5 endpoints are selected manually as the input for the sequence. The first frame of our data is of high image quality, so intermediate point was not needed.

The parameters setting for vessel surface recovering is: $T = 0.4$, $\theta = 0.92$ and $\tau = 0.5$. And the for key point detection and matching: $\eta = 0$, $w_{min} = 2$, $h_{min} = 1.5$ and $\alpha = 0.8$.

The ground truth for each centerline contains a reference centerline and a hand-crafted mask. The mask is generated from a the flux pre-segmented volume with remaining surrounding heart structures and branches eliminated by connected region selection and manual modification. The reference centerline is generated from the mask by a skeleton algorithm based on fast marching [28].

We performed quantitative evaluation in terms of overlap and distance measure. We used the definition of Overlap(OV) in [27] as:

$$OV = \frac{TRM + TPR}{TPM + TPR + FN + FP}$$

where the False Positive(FP) points are determined by the mask. After resampling using a distance of 0.03mm, distance between two centerlines $l_1$and $l_2$is defined as:

$$d(l_1, l_2) = \frac{1}{M+N}\left(\sum_{i=1}^{M} d(l_1(i), l_2) + \sum_{j=1}^{N} d(l_2(j), l_1)\right)$$

The point correspondence is determined by the minimum distance between the points on the two centerlines. False extracted centerline sections are not included in the distance measure.

	OV/ %	AC/mm
Before distal vessel tracking		
LAD	92.97	0.6536
LCX	76.50	0.6541
RCA	94.48	0.6430
After distal vessel tracking		
LAD	93.56	0.6508
LCX	90.96	0.6141
RCA	93.76	0.6297

Discussion

This paper presented a semi-automatic coronary artery segmentation scheme for 3-D CTA sequence. The main coronary centerline extraction method is designed on spherical flux filter and minimal path. The two end points and a few intermediate points are automatically matched starting from the second frame, where a stable landmark key point detection method was proposed. The 3D SIFT descriptor was used for uniquely describing the key points. The overlap measure result are 92.97% (LAD), 76.50% (LCX) and 94.48% (RCA). The accuracy measure result is below the resolution (0.68mm). Due to the failure of matching, especially for LCX, the distal vessel centerlines are easily missed. We proposed a tracking method to complete the extraction. The intensity and radius information was used to improve its robustness. The overlap result was improved to 90.96% for LCX. To build patient-specific vessel model, the vessel represented by its centerline and vessel radius, a simple method was employed to extracted the surface from extracted centerlines.

References

[1] World Cancer Report 2014[J]. World Health Organization, 2015.

[2] Sharp G, Fritscher K D, Pekar V, et al. Vision 20/20: Perspectives on automated image segmentation for radiotherapy[J]. Medical Physics, 2014, 41(5):050902.

[3] Husmann L, Leschka S, Desbiolles L, et al. Coronary artery motion and cardiac phases: dependency on heart rate -- implications for CT image reconstruction. Radiology, 2007, 245(2):567.

[4] Guy Shechter, Frederic Devernay, Ève Coste-Manière, Arshed Quyyumi, Elliot R. McVeigh:Three-Dimensional Motion Tracking of Coronary Arteries in Biplane Cineangiograms. IEEE Trans. Med. Imaging 22(4): 493-503 (2003)

[5] Sarry L, Boire J Y. Three-dimensional tracking of coronary arteries from biplane angiographic sequences using parametrically deformable models[J]. IEEE Transactions on Medical Imaging, 2001, 20(12):1341-51.

[6] Ruan S, Bruno A, Collorec R, et al. 3D Motion and reconstruction of coronary networks Engineering in Medicine and Biology Society, 1992, International Conference of the IEEE. IEEE, 1992:2048-2049.

[7] John Puentes, Christian Roux, Mireille Garreau, Jean-Louis Coatrieux: Dynamic Feature Extraction of Coronary Artery Motion using DSA Image Sequences. IEEE Trans. Med. Imaging 17(6): 857-871 (1998)

[8] Guanyu Yang, Jian Zhou, Dominique Boulmier, Marie-Paule Garcia, Limin Luo, Christine Toumoulin: Characterization of 3-D coronary tree motion from MSCT angiography. IEEE Trans. Information Technology in Biomedicine 14(1): 101-106 (2010)

[9] Dong Ping Zhang, Laurent Risser, Coert Metz, Lisan Neefjes, Nico Mollet, Wiro J. Niessen, Daniel Rueckert: Coronary artery motion modeling from 3D cardiac CT sequences using template matching and graph search. ISBI 2010: 1053-1056

[10] David Lesage, Elsa D. Angelini, Isabelle Bloch, Gareth Funka-Lea: A review of 3D vessel lumen segmentation techniques: Models, features and extraction schemes. Medical Image Analysis 13(6): 819-845 (2009)

[11] Cemil Kirbas, Francis K. H. Quek: A review of vessel extraction techniques and algorithms. ACM Comput. Surv. 36(2): 81-121 (2004)

[12] Matthias Schneider, Sven Hirsch, Bruno Weber, Gábor Székely, Bjoern H. Menze: Joint 3-D vessel segmentation and centerline extraction using oblique Hough forests with steerable filters. Medical Image Analysis 19(1): 220-249 (2015)

[13] Alejandro F. Frangi, Wiro J. Niessen, Koen L. Vincken, Max A. Viergever: Muliscale Vessel Enhancement Filtering. MICCAI 1998: 130-137
[14] Max W. K. Law, Albert C. S. Chung: Efficient Implementation for Spherical Flux Computation and Its Application to Vascular Segmentation. IEEE Trans. Image Processing 18(3): 596-612 (2009)
[15] M. Sabry Hassouna, Aly A. Farag: MultiStencils Fast Marching Methods: A Highly Accurate Solution to the Eikonal Equation on Cartesian Domains. IEEE Trans. Pattern Anal. Mach. Intell. 29(9): 1563-1574 (2007)
[16] Blaine Rister, Mark A. Horowitz, Daniel L. Rubin: Volumetric Image Registration From Invariant Keypoints. IEEE Trans. Image Processing 26(10): 4900-4910(2017)
[17] Dijkstra E W. A Note on Two Problems in Connection with Graphs[J]. Numerische Mathematics, 1959, 1(1):269--271.
[18] Fethallah Benmansour, Laurent D. Cohen: Tubular Structure Segmentation Based on Minimal Path Method and Anisotropic Enhancement. International Journal of Computer Vision 92(2): 192-210 (2011)
[19] Metz C T, Schaap M, Weustink A C, et al. : Coronary centerline extraction from CT coronary angiography images using a minimum cost path approach. Medical Physics, 2009, 36(12): 5568-5579.
[20] Ning Zhu, Albert C. S. Chung: Graph-Based Optimization with Tubularity Markov Tree for 3D Vessel Segmentation. CVPR 2013: 2219-2226
[21] Noha Youssry El-Zehiry, Leo Grady: Vessel segmentation using 3D elastica regularization. ISBI 2012: 1288-1291
[22] Alice Dufour, Nicolas Passat, Benoît Naegel, Joseph Baruthio: Interactive 3D brain vessel segmentation from an example. ISBI 2011: 1121-1124
[23] Hua Li, Anthony J. Yezzi: Vessels as 4-D Curves: Global Minimal 4-D Paths to Extract 3-D Tubular Surfaces and Centerlines. IEEE Trans. Med. Imaging 26(9): 1213-1223 (2007)
[24] David Lesage, Elsa D. Angelini, Isabelle Bloch, Gareth Funka-Lea: Design and Study of Flux-Based Features for 3D Vascular Tracking. ISBI 2009: 286-289
[25] Alexander Vasilevskiy, Kaleem Siddiqi: Flux Maximizing Geometric Flows. IEEE Trans. Pattern Anal. Mach. Intell. 24(12): 1565-1578 (2002)
[26] David G. Lowe: Distinctive Image Features from Scale-Invariant Keypoints. International Journal of Computer Vision60(2): 91-110 (2004)
[27] Michiel Schaap, Coert Metz, Theo van Walsum, Alina G. van der Giessen, Annick C. Weustink, Nico Mollet, Christian Bauer, Hrvoje Bogunovic, Carlos Castro-Gonzalez, Xiang Deng, Engin Dikici, Thomas O'Donnell, Michel Frenay, Ola Friman, Marcela Hernández Hoyos, Pieter H. Kitslaar, Karl Krissian, Caroline Kühnel, Miguel A. Luengo-Oroz, Maciej Orkisz, Örjan Smedby, Martin Styner, Andrzej Szymczak, Hüseyin Tek, Chunliang Wang, Simon K. Warfield, Sebastian Zambal, Yong Zhang, Gabriel P. Krestin, Wiro J. Niessen: Standardized evaluation methodology and reference database for evaluating coronary artery centerline extraction algorithms. Medical Image Analysis 13(5): 701-714 (2009)
[28] Van Uitert R, Bitter I. Subvoxel precise skeletons of volumetric data based on fast marching methods[J]. Medical Physics, 2007, 34(2):627.